ELSEVIER

Erosion–corrosion of mild steel in hot caustic. Part I: NaOH solution

Rihan Omar Rihan, Srdjan Nešić [*]

The Department of Mechanical Engineering, University of Queensland, Brisbane, Qld 4000, Australia

Abstract

A novel apparatus, high-pressure/high-temperature nickel flow loop, was constructed to study the effect of the flow on the rate of erosion–corrosion of mild steel in hot caustic. It has been successfully used to measure the corrosion rate of 1020 steel in 2.75 M NaOH solution at a temperature of 160 °C and velocities of 0.32 and 2.5 m/s. In situ electrochemical methods were used to measure the corrosion rate such as the potentiodynamic sweep, the polarization resistance method, and electrochemical impedance spectroscopy (EIS). Also used were the weight-loss method and scanning electron microscopy (SEM).

Eight electrodes/coupons were used to monitor the metal loss rate, four were placed at the low velocity section, while the other four were placed in the high velocity section. The first three coupons in each section were placed within the disturbed flow region, while the fourth was placed in a fully developed flow region.

The corrosion rate of the coupons in the high velocity section was generally higher than that of the coupons in the low velocity section. One coupon in the disturbed flow region had a significantly higher corrosion rate than the others.

© 2005 Elsevier Ltd. All rights reserved.

[*] Corresponding author. Tel.: +1 740 593 9945; fax: +1 740 593 9949.
E-mail address: nesic@ohio.edu (S. Nešić).

1. Introduction

Many bauxite refineries utilize what is known as the ''Bayer process'' in the production of aluminium oxide (alumina), a process involving a strong caustic solution. At a particular stage in the process, the caustic solution is passed through a series of heat exchangers in order to recuperate heat. The headers of these heat exchangers which are constructed of mild steel are regularly inspected for corrosion damage. Long term data collection has indicated localized corrosion damage to certain sections of the heat exchangers' header shells and tube-sheets. The damage appeared to be flow related.

Erosion–corrosion is a type of attack predominantly observed on mild steel, displaying active-passive behaviour in caustic solutions due to formation of surface films. In order to operate mild steel equipment in caustic environments, it is essential that these protective surface films do form and survive the operating conditions. The protective surface films protect the bare metal from a high corrosion rate by providing a ''barrier'' between the solution and the bare metal. It is believed that these films can be removed completely or partially under certain water chemistry and flow conditions, such as disturbed turbulent flow. Once the protective surface films are removed or damaged, the bare metal becomes exposed directly to the solution and a severe localized corrosion and failure of the equipment may occur. This type of attack is commonly referred to as: flow affected corrosion (FAC) or erosion–corrosion. In this context, the word *erosion* refers to a hydro-mechanical removal of the protective film by the flow while the main mode of metal loss is due to *corrosion*.

Erosion–corrosion often occurs at the heat exchanger tube inlets, where the flow experiences a sudden contraction as it moves from the large cross-sectional area of the heat exchanger header into the small cross-section area of the tubes. The sudden contraction of the flow at the tube inlets causes a flow disturbance, which can remove the protective surface films partially or completely, thus causing severe localized erosion–corrosion, and subsequent failure. The available literature on the corrosion of mild steel in caustic is very limited, especially at high-temperatures and high-pressures.

It is generally accepted that in alkaline solutions the overall corrosion reaction is [1]:

$$3Fe + 4H_2O \rightarrow Fe_3O_4 + 4H_2 \tag{1}$$

In other words the final product of this reaction, which is electrochemical in nature, is magnetite Fe_3O_4 usually found on the surface of the steel. The exact mechanism of this reaction is difficult to pinpoint as there is a number of possible pathways.

1.1. Cathodic reaction

The concentration of hydrogen ions is very low in highly alkaline deoxygenated solutions so the cathodic current comes primarily from direct reduction of water (dragging away of the OH^- portion of the adsorbed water molecules) [1]:

$$2H_2O + 2e^- \rightarrow H_2 + 2OH^- \tag{2}$$

1.2. Anodic reaction

One can assume the following anodic reaction dominates in alkaline solutions:

$$Fe + 2OH^- \rightarrow Fe(OH)_2 + 2e^- \tag{3}$$

The solid ferrous hydroxide film is in equilibrium with a number of dissolved ferrous species[1] such as: $Fe^{2+}, FeOH^+, Fe(OH)_3^-, HFeO_2^-, FeO_2^{2-}$. The concentration of these species is defined by a set of chemical equilibria and the alkalinity of the solution. For example in alkaline solutions the reaction:

$$HFeO_2^- + OH^- \iff FeO_2^{2-} + H_2O \tag{4}$$

has the equilibrium moved far to the rhs of the reaction. Hence, the main dissolved species is ferroate (hypoferrite) FeO_2^{2-} which is in equilibrium with the ferrous ions:

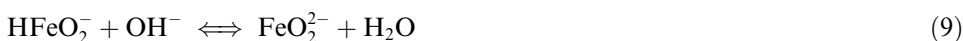$$FeO_2^{2-} + 2H_2O \iff Fe^{2+} + 4OH^- \tag{5}$$

There is no need to list here all the equilibrium reactions as they are available in the open literature [3]. Another way to write an overall anodic reaction for alkaline solutions is:

$$Fe + 2H_2O \iff HFeO_2^- + 3H^+ + 2e^- \tag{6}$$

or in terms of a mechanism:

$$Fe + H_2O \iff FeOH_{ads} + H^+ + e^- \tag{7}$$

$$FeOH_{ads} + H_2O \xrightarrow{rds} HFeO_2^- + 2H^+ + e^- \tag{8}$$

followed by the equilibrium

$$HFeO_2^- + OH^- \iff FeO_2^{2-} + H_2O \tag{9}$$

1.3. Passivity

The word *passive* in the present context can be somewhat misleading as it is usually associated with the *passive* behavior of stainless steel and very low corrosion rates. Although the form of the polarization sweeps obtained on mild steel in high-temperature caustic solutions does show a active/passive transition peak [4,5], the obtained *passive* current is frequently of the order of 1 A/m^2 or even higher. This corresponds to corrosion rates of 1 mm/y and higher for steel and in most practical cases, when mild steel corrodes at such a high rate, it can be misleading to characterise this behavior as *passive*. However, since the term *passive* has been used extensively in the literature, it has been adopted here as well, in order to avoid confusion.

The onset of *passivity* of mild steel in alkaline solutions is most often related to formation of a protective film on the steel surface. In de-oxygenated alkaline solution it is most likely that the surface film will be composed of magnetite Fe_3O_4. There are a few proposals suggesting different mechanisms for this process.

The *precipitation model* [1] assumes that once the concentration of ferrous species becomes sufficiently high, the solubility product of magnetite will be exceeded, leading to deposition of a surface film. The relevant reversible dissolution/precipitation chemical reactions describing this process can be written in a compact form as [6]:

$$3Fe(OH)_b^{(2-b)+} + (4-3b)H_2O \iff Fe_3O_4 + 3(2-b)H^+ + H_2(g) \tag{10}$$

---
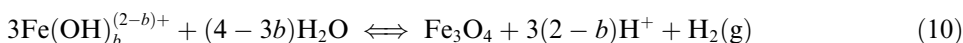
[1] According to some studies [2] the presence of ferric species such as $Fe^{3+}, Fe(OH)_3, Fe(OH)_4^-$ in deoxygenated solutions can be neglected in the potential range of interest so they will be omitted from the present discussion.

where the integer parameter $b = 0, 1, 2, 3$ is used to denote the different iron species, e.g. 0 refers to Fe^{2+}, etc.

The protectiveness of such a film will depend on its structure and porosity which is influenced by a number of factors such as nucleation rate, supersaturation level, electrochemical potential, state of the surface, presence of other species in the solution, etc. Very little is known on the relationship between these factors and the protectiveness of a surface film.

Another theory [7] proposes that the onset of passivity of mild steel in alkaline solutions is related to *direct* oxidation of the $HFeO_2^-$ via:

$$3HFeO_2^- + H^+ \rightarrow Fe_3O_4 + 2H_2O + 2e^- \tag{11}$$

forming an adherent, non-porous Fe_3O_4 film offering good protection. Other proposals [8] include *direct* oxidation of Fe to form a protective Fe_3O_4 film according to Eq. (1).

Finally, it has been generally accepted that an important path for forming magnetite film is the so called "Schikorr's reaction":

$$3Fe(OH)_2 \rightarrow Fe_3O_4 + H_2(g) + H_2O \tag{12}$$

It is quite possible that the growth of the magnetite film proceeds according to several mechanisms simultaneously. The proposal that the film grows from the inner (metal interface) side via the *direct* oxidation mechanism, while it grows from the outside (solution interface) side via the *precipitation* mechanism seems plausible as it leads to a "duplex" film structure often observed in experiments [8]. In these films, due to the confined space, the inner layer consists of a small-grain, low-porosity crystal structure, while the outer layer consists of larger, free-growing crystallites with higher porosity. It has been reported [9,10] that the inner compact layer firmly adhering to the surface is the one offering protection while the outer porous layer was less protective and vulnerable to removal by flow.

1.4. Loss of passivity

From the results scattered throughout the reports it became quite clear that certain factors influence the corrosion rate by affecting the survival of the protective surface films. For example it is generally known that high velocity leads to higher film removal rate either through a *dissolution* or a mechanical *erosion* mechanism.

- *Dissolution* film removal mechanism is commonly accepted and most often controlled by the mass transfer through the liquid boundary layer. The rate of this process depends on the chemistry of the solution and the local near wall turbulence levels. Turbulence levels can vary significantly particularly in complex flow geometries such as pipe inlets, valves and in all other cases where disturbed flow conditions are present.
- *Erosion* film removal mechanism is far less understood although it cannot be excluded as a possibility. It can only be speculated that high near-wall turbulence levels and/or mean wall shear stress can lead to film mechanical erosion or, what is more probable, interfere with film formation. The feasibility of this proposal, and even more so the exact mechanism for this process, is unknown. It was reported that the contribution of the dissolution mechanism can be additive to film erosion and sometimes even act in a synergistic way by loosening the crystal grains of the film making them more prone to erosion [11,12].

Meyer and Atrens [13] examined tubes inlets from Bayer heat exchangers to characterise service erosion–corrosion. Three distinct regions were observed: the thin wall region, which extends from the tube inlet to a distance of approximately one tube diameter, had a smooth, wavy surface with some localized wall perforation; the transition region, which starts at a distance of approximately one tube diameter from the tube inlet, had a valley morphology; and the thick wall area, starting at a distance of approximately one to two diameters from the tube inlet, which had pits and horseshoes. Therefore, in this project, the tube's inlet region was fully covered by inserting three working electrodes downstream from a sudden pipe constriction in order to measure the corrosion rate at these three critical positions. Meyer et al. [14] used the impinging-jet test rig to study the mechanism of the erosion–corrosion of caustic solution at high-temperatures used at a Bayer plant site. When the liquid jet was submerged under controlled conditions, the observed damage rates were low for all conditions of one-phase flow. The presence of particulates in the Bayer liquor had no significant effect on the erosion–corrosion rates. Higher damage rates were measured by using liquor at higher temperatures. It appeared that in single-phase flow the rate of erosion–corrosion remains low, a fact not confirmed in the present study as shown below. It can be speculated that the low rates of attack observed by Meyer et al. [14] were related in the first place to the startup procedures used in their experiments. Meyer and Atrens [15] tested the effect of the composition of Bayer liquor, the nature of the localized attack, the presence of atmospheric gases (O_2 and N_2), and two-phase flow. The presence of atmospheric gas bubbles (O_2 and N_2) caused damage to the coupons. Two-phase liquid–vapour flow caused high damaged rates, while the single-phase liquid flow had low erosion–corrosion damage rates under all conditions.

May and Orchard [16] and May [17] studied the corrosion of carbon steel exposed to spent Bayer liquor and analysed the relative effects of process variables, erosion–corrosion, stress corrosion, and inhibitors and microstructure on the rate of general corrosion. They found that the corrosion resistance depends on surface passivation and material microstructure. At velocities less than 2.5 m/s, erosion is not an important metal removal mechanism, but at velocities more than 4 m/s rapid degradation may occur [16,17]. Therefore, it was expected that for the velocities used in the present project ($\leqslant$2.5 m/s) there should be only a limited effect of velocity on the rate of erosion–corrosion.

Flis et al. [18] studied the effect of non-de-aerated 8.5 M NaOH at 100 °C on stagnant decarbonised iron and its alloys with 0.23 wt.% C and 0.875 wt.% C. Flis et al. [18] concluded that iron showed a higher tendency for passivation than these alloys, the formation of the passive film on iron was easier than on the alloys, and its stability was higher than on the alloys. From these results, Flis et al. [18] concluded that carbon retards the passivation of iron in hot NaOH and weakens the stability and compactness of the passive film. Yasuda et al. [19] investigated the effect of 30% and 50% NaOH at boiling temperatures (117 °C and 148 °C, respectively) on stagnant carbon steel, austenitic stainless steels, nickel alloys, and nickel. The corrosion rate of these alloys in boiling caustic solution was greater than that in the hydrogen-saturated solution at the same temperature and concentration. Increasing the nickel content in the alloy decreased the corrosion rate. Ogata et al. [20] studied the effect of 2–20 M NaOH at temperatures 50–200 °C under a pressure of 20 atm on stagnant iron, nickel, and Raney nickel. The corrosion rate of iron in hot

concentrated caustic was high, while nickel had a high corrosion resistance to caustic. Sriram and Tromans [7] studied the effect of de-aerated caustic aluminate solutions on stagnant 0.18 C steel at 92 °C. The anodic dissolution of the steel was inhibited by the presence of AlO_2^- anions.

Studying the effects of turbulent flow on corrosion was commonly performed by using rotating cylinder electrodes [21,22]. Rotating cylinder electrodes have been used in previous studies on corrosion and/or protective film formation close to room temperature [23–27] or at high-temperature close to or more than 100 °C [4,28]. Stationary electrodes were used at a high-temperatures in non-mixed solutions [29–34]. Meyer and Atrens [35] inserted probes into a Bayer plant's heat exchanger train. Newton et al. [36] developed an in situ corrosion monitoring system for high-temperature Bayer solution operation up to 240 °C.

Bremhorst and Lai [37] studied the role of flow characteristics on the erosion–corrosion of the tube inlets in the inlet channel of shell and tube heat exchangers handling solutions with some solid content. Different flow patterns were investigated. Cross-flow, which existed in the header near the tube ends, was primarily the cause of the erosion–corrosion. Different flow correction devices have been tested and their effect on the flow pattern in the header have been observed and evaluated by Lai and Bremhorst [38]. The best flow corrector device providing the most favorable flow pattern was the perforated plates. Due to impracticalities of this design a prism attached to the baffle was selected as the solution which was implemented in the heat exchanger headers. Bremhorst and Flint [39] identified flow patterns, particularly flow impingement angles, in several sections of a standard multipass shell and tube heat exchanger. These results were compared with the observed tube wear in a plant. The similarity between high metal loss and large flow incidence angle was close.

One can conclude that despite some progress, the mechanism of erosion–corrosion in caustic solutions involving the formation and removal of protective oxide films is still largely unknown.

2. Experimental equipment

The apparatus used in this experimental work was a high-pressure/high-temperature nickel flow loop. The design and building of the high-pressure/high-temperature nickel flow loop was an integral part of the present project and required a major effort. The high-pressure/high-temperature nickel flow loop is illustrated in Fig. 1.

The loop can handle temperatures up to 300 °C and pressures up to 200 bar. All the wetted parts of the loop are made from pure nickel and high-nickel containing alloys such as Monel 400, Hastelloy C, and Inconel 601, and Teflon since these materials have an excellent erosion–corrosion resistance to hot caustic solution. The piping of the loop is 1/2 in. nominal diameter nickel pipe. The main components of the loop are described below.

The test section is the most important part of the loop. It is made from nickel. The test section was designed to simulate the disturbed flow conditions present in the heat exchangers and indeed to house the coupons. The test section is made from four major components joined together by two stainless steel flanges (see Fig. 2). The test section is mounted vertically in order to prevent the entrapment of gases particularly in the large-diameter section. The main parts of the test section are:
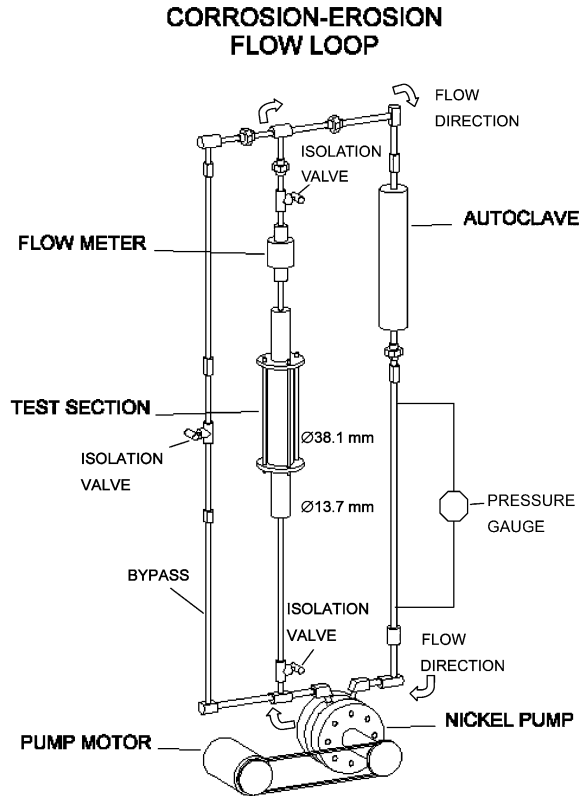
Fig. 1. A sketch of the high-pressure/high-temperature nickel flow loop.

- *The large-diameter section.* As the flow enters the test section it passes through a sudden diameter expansion which roughly approximates the flow entering the heat exchanger header. A straight section of pipe 40-pipe diameters in length was installed upstream of the entire test section in order to ensure fully developed flow entering the test section. The internal diameter of the inlet pipe to the large-diameter section part is ∅13.7 mm while the large-diameter section part it is ∅38.1 mm giving a 1:9 expansion area ratio. The length of the large-diameter section is 500 mm.
- *The small-diameter section.* From the large-diameter cross-section, the flow enters the small-diameter cross-section (sudden pipe constriction) as illustrated in Fig. 2. The length of the small-diameter section is 300 mm and its diameter is ∅13.7 mm. This part of the test section broadly approximates the disturbed flow situation present at the inlet of the heat exchanger tubes.
- *Working electrodes.* There are eight coupons (working electrodes) inserted at different positions through the test section as illustrated in Fig. 2. Four electrodes are inserted in the large-diameter section, and four more in the small-diameter section. Three electrodes in each section are placed in the disturbed flow region. The fourth electrode in each section is placed as far from the disturbed flow region as possible, where the flow has recovered. Each electrode is given a number as shown in Fig. 2. The working electrodes are made from the material to be tested in the present project, which is 1020 mild
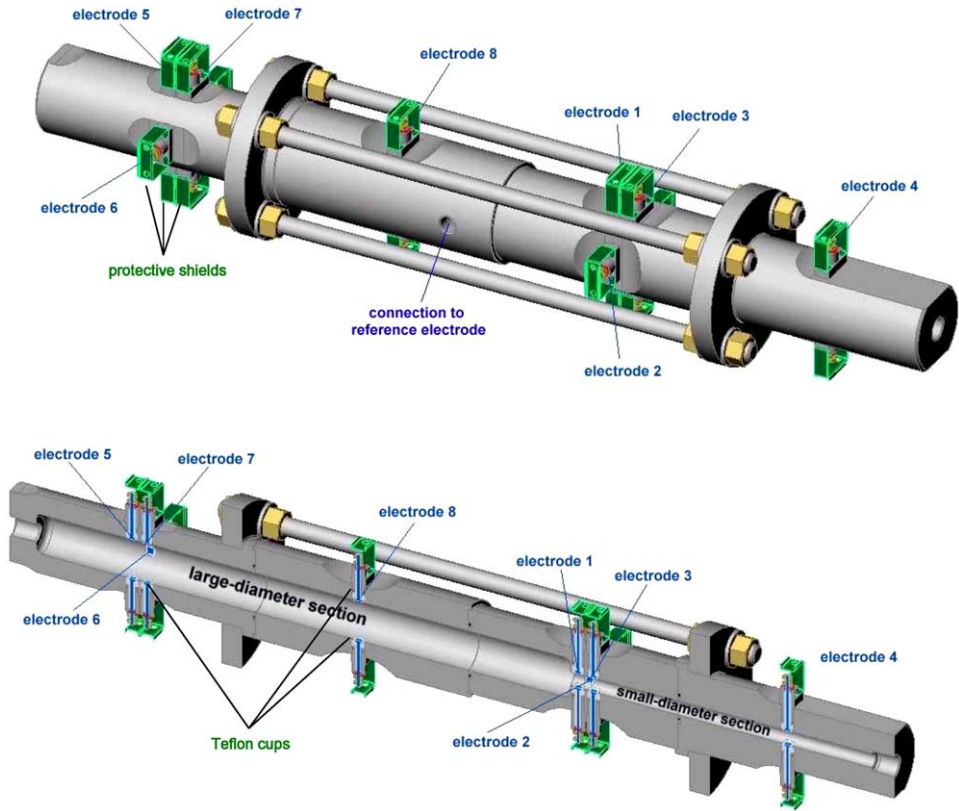
Fig. 2. The outside and the cross-section views of the test section showing the positioning of the working electrodes (coupons).

steel. The chemical composition of 1020 mild steel is illustrated in Table 1 expressed in wt.%.

- *Counter electrodes.* For the purpose of electrochemical measurements there are eight counter electrodes (see Fig. 2). They are placed diametrically opposite to the working electrodes in order to ensure a symmetrical current distribution during electrochemical polarization measurements. The counter electrodes are made from Inconel 601, as this material has an excellent resistance in hot caustic solution. The counter electrodes are the same size and shape as the working electrodes. The working and counter electrodes are enclosed in Teflon cups to avoid contact with the test section body as illustrated in Figs. 2 and 3. Teflon was chosen because of its excellent corrosion resistance to almost all chemicals. Also, it can withstand temperatures as high as 310 °C.

Table 1
The chemical composition of 1020 mild steel coupons expressed in weight percent

C	P	Mn	Si	S	Ni	Cr	Mo	Cu	Fe
0.21	0.027	0.82	0.01	0.018	0.02	0.03	0.01	0.01	Balance
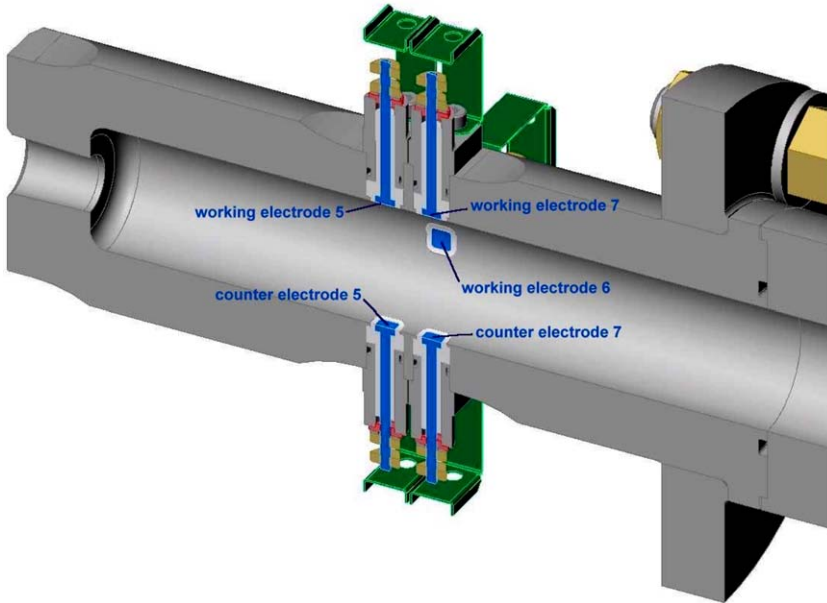
Fig. 3. Electrodes (coupons) position detail in the large-diameter section.

The working and counter electrodes are protected by safety shields, as shown in Figs. 2 and 3, to prevent the electrode stems from being expunged as projectiles in the unlikely case the head of the electrodes completely corrode and/or fail mechanically.

- *Reference electrode.* There is only one external Ag/AgCl reference electrode attached to the test section. In most of the experiments a simple Ag rod (2 mm diameter and 45 mm long) coated by AgCl which was prepared by anodically polarizing the Ag rod in a saturated KCl solution at room temperature. A current density of 10 mA/cm^2 was used for 3 min in order to coat the rod with a durable AgCl layer. In the experiments the reference electrode was continuously wetted by the solution which was extracted from the test section and cooled to room temperature, by passing through a small cooler.

The turbine pump is used to circulate the solution through the loop. The wetted parts of the pump are made from nickel 200. The pump is sealed by two teflon encapsulated viton O rings, which can handle temperatures up to 230 °C. The pump has a maximum head differential of 103 kPa at 19 l/min and 25 °C. The design pressure is 34.5 MPa at 300 °C, and the hydrostatic test pressure is 51.7 MPa at 25 °C.

The tank (autoclave) is a 2 l pressure vessel acting as a reservoir for the solution surrounded by three electric band heaters which heat the solution. It is equipped with a level indicator to indicate the level of the solution inside the autoclave, a pocket to house a thermocouple to measure the temperature of the solution inside the autoclave and a nitrogen gas connection.

There is a flow line parallel to the test section line as illustrated in Fig. 1. It is used to pass the solution through the loop during the heating process taking place (while the test section line is closed). Once the required temperature is reached, the test section line is

opened in order to expose the coupons directly to the solution at the required temperature (while the bypass line is closed).

The dosing pump can be used to pump additional solution into the loop during the experiment at high-pressure if needed. Topping-up of the loop with the working solution or adjustment of the solution composition during the experiment are two examples.

The magnetic flowmeter has a wafer style flow tube lined with perfluoroalkoxy (PFA). It has two Hastelloy C electrodes. The internal nominal diameter of the flowmeter tube is 15 mm. The flowmeter measurement range is 0.01–10 m/s. It can stand a maximum temperature of 180 °C, and a maximum pressure of 4.5 MPa at 180 °C.

A pressure transducer is used to measure the total pressure inside the loop. The sensor is made from Hastelloy C, and the body of the transducer is filled with silicon oil. The span limits of the pressure transducer are 0.7–21 MPa. It is equipped with a liquid crystal display. The differential pressure transducer is used to measure the pressure drop between two points along one of the loop's straight pipe sections. The measured pressure drop can be used to calculate the velocity, which is an alternative way to measure the flow rate (in addition to the flowmeter). The sensor is made from Hastelloy C, and the body is filled with silicon oil. The differential pressure transducer has span limits of 0.12–7.5 kPa, and range limits of −7.5 to 7.5 kPa. It is equipped with a liquid crystal display.

A potentiostat is used to monitor the corrosion rate on line. The potentiostat boards inserted into a PC have the following specifications; maximum current ±300 mA, minimum current ±3 nA, maximum potential ±12 V, minimum potential ±0.03 V, and measures an impedance of 10^9 ohms or higher. The multiplexer is attached to the potentiostat and is used to log sequentially and continuously the corrosion rate of all the eight working electrodes according to a prescribed program.

Since typical experiments lasted about three days, it was essential to log and control the process variables such as velocity, temperature, pressure and differential pressure, by using data acquisition and control software. All the relevant parameters were logged every 10 min.

3. Results and discussion

In all the experiments, the following experimental methods were used:

- Polarization resistance method—used to measure the corrosion rate in situ at different time intervals during the experiment.
- Potentiodynamic sweep—primarily used to obtain an indication of the corrosion mechanisms and determine the Tafel slopes for the anodic and cathodic reaction.
- Electrochemical impedance spectroscopy—attempted in order to measure in situ the polarization resistance at different time intervals during the experiment as an alternative to the Polarization resistance method and also to help identify the corrosion mechanism.
- Weight loss—used to calculate the time-averaged corrosion rate during the experiment.
- Scanning electron microscopy—used to investigate the appearance of the corrosion surface and to check for presence of the protective surface film.

This experimental series was named "Experiment 1.1" and the same experiment was repeated three times. The individual repeats are designated as 1.1-1, 1.1-2, and 1.1-3.

Table 2
The conditions for Experiment 1.1

Temperature (°C)	Mean velocity (m/s)	
	Small-diameter pipe section	Large-diameter pipe section
160	2.5	0.32

The reference electrode used in Experiments 1.1-2 and 1.1-3 was a laboratory prepared Ag/AgCl reference electrode as previously described. In Experiment 1.1-3, a commercial Ag/AgCl reference electrode was tested.

The electrolyte used in Experiment 1.1 was made by dissolving 2.75 M NaOH and 1.5 wt.% NaCl in de-aerated distilled water. The selected concentration of NaCl was chosen to be similar to the concentration in actual Bayer solution [17]. Both chemicals, NaOH and NaCl, were analytical reagents (AR) grade.

Other experimental conditions are summarized in Table 2.

The experimental procedure was as follows:

- The coupon were prepared by grinding with 1500/2000 grit paper, then washed by ethanol and allowed to dry. They were weighed before being installed in the test section, in order to calculate the weight loss.
- The loop was flushed with nitrogen gas to get the oxygen out of the loop.
- The test section was closed and the loop was filled with previously de-aerated caustic solution.
- The caustic solution was circulated and simultaneously heated to 160 °C.
- The test section was opened and the by-pass line was closed.
- The electrochemical measurements were started.
- After completion of the experiments the coupons were removed from the test section and immediately washed with ethanol. They were then dried and stored in a desiccator. The corrosion products were removed as described below.

3.1. Potentiodynamic sweep measurements

This method was used only in Experiment 1.1-1 to investigate the corrosion mechanism of 1020 mild steel in hot caustic solution and to estimate the anodic and cathodic Tafel slopes. A typical potentiodynamic polarization curve (taken at electrode 7) is illustrated in Fig. 4. The scan rate used was 0.2 mV/s. It is obvious the working electrode displays an active-passive behaviour. The parts of the curves closer to the free corrosion potential were used to calculate the Tafel slopes, since they show distinct linear regions particularly on the cathodic side. The linearity of the anodic portion of the polarization curves was not as pronounced. The calculated values of the Tafel slopes are illustrated in Table 3.

The values of the cathodic Tafel slopes were reasonably consistent. On the other hand a broad variation was obtained for the anodic Tafel slopes at different electrodes depending on whether the electrodes were corroding actively or not. In order to obtain an average anodic Tafel slope the values obtained for electrodes 4 and 8 were excluded as they indicated pre-passive behaviour. All the cathodic Tafel slopes were used for averaging. As a result, the average values of the Tafel slopes were 44 mV/decade for the anodic and
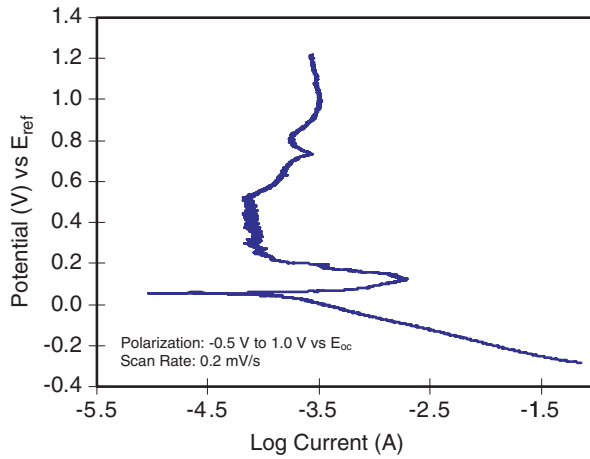
Fig. 4. A typical potentiodynamic sweep curve obtained in Experiment 1.1-1 for electrode 7.

Table 3
Estimated Tafel slope values for different electrode positions

Electrode Number	b_a (mV/decade)	b_c (mV/decade)
1	47	143
2	37	133
3	48	150
4		137
5	34	117
6	55	129
7	43	125
8		128
Average value	44	133

133 mV/decade for the cathodic reaction. It is believed that these can be attributed to active iron dissolution reaction (3) and water reduction reaction (2) respectively. These values of anodic and cathodic Tafel slopes were used for all the experiments where active iron dissolution was observed in order to calculate the **B** value needed for conversion of the polarization resistance into a corrosion rate. For electrodes displaying passive behaviour, a value of infinity for the anodic Tafel slope was used to calculate the **B** value. As a comparison it is worth noticing that the cathodic Tafel slope used by Ogata et al. [20] was 175 mV/decade for 99.5% pure iron in 10 m NaOH at 150 °C. Yasuda et al. [19] estimated the anodic and cathodic Tafel slopes to be 45 and 165 mV/decade, respectively, for different metals and alloys including iron in 30% and 50% NaOH at boiling temperatures of 117 °C and 148 °C, respectively.

The Tafel analysis of the potentiodynamic sweep was an unreliable method for calculation of the corrosion rate, since the corroding surface was perturbed significantly by the high polarization applied. It initially appeared that Tafel analysis based on this method gave much higher corrosion rate values than the polarization resistance method. This difference in corrosion rate could be clearly related to the shift in corrosion potential (E_{corr})
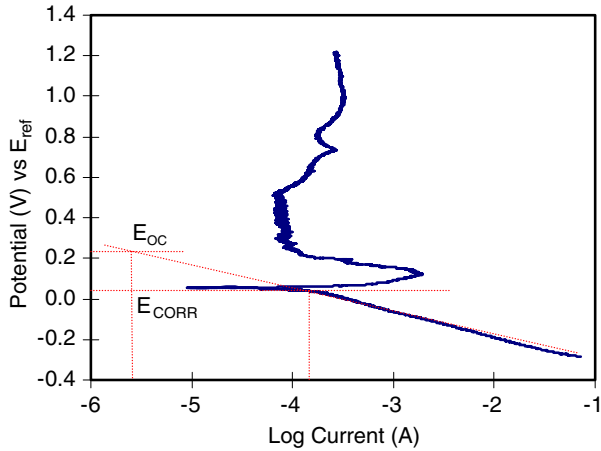
Fig. 5. The shift in the open-circuit/corrosion potential before (E_{oc}) and after the potentiodynamic sweep (E_{corr}).

before and after the potentiodynamic sweep as illustrated in Fig. 5. It can be seen that the open circuit potential (E_{oc}) recorded prior to the sweep was more noble than the corrosion potential (E_{corr}) recorded during the sweep. Since the polarization sweep was conducted by sweeping the potential from cathodic to anodic potentials, most likely the protective films were reduced in this process, resulting in a lower corrosion potential and a much higher corrosion rate. The shift in the corrosion potential varied between 135 and 200 mV across the eight electrodes.

3.2. Polarization resistance measurements

This method was used to obtain the polarization resistance R_p from the slope of the potential/current curve. Most of the measurements were done by polarizing the working electrode starting at 20 mV below and ending 20 mV above the open circuit potential. The scan rate used was 0.1 mV/s. A typical polarization curve is illustrated in Fig. 6.

In Experiments 1.1-1, 1.1-2, and 1.1-3, some electrodes showed "linearity" (electrodes 2, 3, and 4) as shown in Fig. 6, and the other showed non-linearity as shown in Fig. 7. The corrosion resistance R_p of the non-linear curves was calculated by drawing a tangent line to the polarization curve at the corrosion potential E_{corr} [40,41]. The slope of this tangent line is the corrosion resistance R_p. The corrosion current (i_{corr}) was calculated by using:

$$i_{corr} = \frac{\mathbf{B}}{R_p} \tag{13}$$

where i_{corr} is the corrosion current density in A/m^2; R_p is the polarization resistance in $\Omega\,m^2$ and $\mathbf{B}$ is the proportionality constant in V/decade:

$$\mathbf{B} = \frac{b_a b_c}{2.3(b_a + b_c)} \tag{14}$$

where b_a is the anodic Tafel constant in V/decade, and b_c is the cathodic Tafel constant in V/decade.
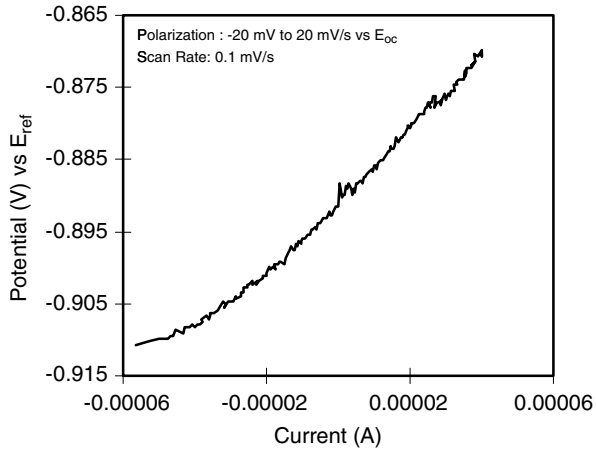
Fig. 6. A typical "linear" polarization resistance curve obtained during the caustic period of Experiment 1.1-1 for electrode 2.
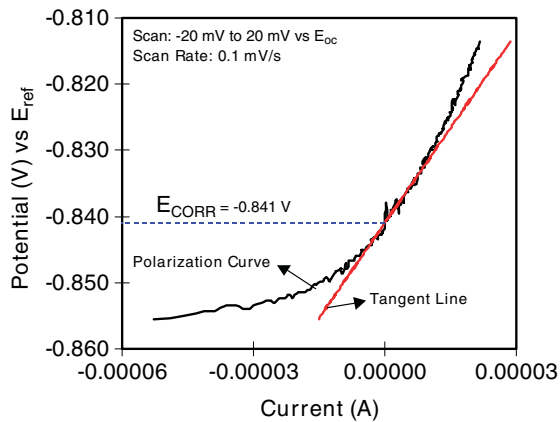

Fig. 7. A typical non-linear polarization curve obtained during the caustic period of Experiment 1.1-1 for electrode 1.

The corrosion rate (CR_{ec}) measured by the electrochemical method was calculated by using:

$$CR_{ec} = \frac{i_{corr} w}{\rho F} \tag{15}$$

where w is the equivalent weight of Fe; F is the Faraday constant, and ρ is the density of Fe.

3.3. Weight-loss measurements

After completion of experiments the mild steel working electrodes (coupons) were removed from the test section and immediately washed with ethanol. They were then dried

and stored in a desiccator. The corrosion products were removed using a standard procedure [42] involving cathodic polarization with a current density of 100 A/m² for 5 min at a temperature of 20–25 °C in a solution made from 100 g diammonium citrate $((NH_4)_2HC_6H_5O_7)$ in 1000 ml reagent water. The anode used was stainless steel. The above procedure was repeated and the electrodes dried and weighed after each time until the weight stopped changing. Since a stainless steel anode was used instead of platinum or carbon, the solution was changed after each cleaning sequence because the stainless steel anode contaminated the solution.

The time-averaged corrosion rate determined by weight loss CR_{wl} in mm/y was calculated by using [43]:

$$CR_{wl} = \frac{K \times W}{A \times T \times \rho}$$

where $K = 8.76 \times 10^6$ (mm/m)(h/y) $= 10^3$ mm/m $\times$ 365 day/y $\times$ 24 h/day is a unit conversion constant; T is the time of exposure in h; A is the exposed area of the electrode in m²; W is the mass loss in kg and ρ is the density in kg/m³.

The time-averaged corrosion rate obtained from electrochemical (polarization resistance) measurements CR_{ec} in mm/y was calculated by using:

$$CR_{ec} = \frac{\sum_i T_i \times CR_i}{\sum_i T_i}$$

where T_i is the measuring time interval in h, and CR_i is the average corrosion rate recorded during that time interval in mm/y.

The comparison of time-averaged corrosion rates obtained by weight-loss and electrochemical measurements is given in Table 4. As can be seen there were significant differences between the corrosion rates calculated by using the weight-loss and the electrochemical (polarization resistance) measurements. Most likely these can be related to an inadequate cleaning procedure used in this series of experiments to remove surface film from the electrode surfaces prior to weight-loss measurements. It has been found that in some cases the corrosion products were not removed entirely (Experiments 1.1-1 and 1.1-3) while in other cases some of the base metal was removed along with corrosion

Table 4

Experiment 1-1: comparison of time-averaged corrosion rates obtained by using electrochemical CR_{ec} and weight-loss measurements CR_{wl}

Electrode number	Experiment 1.1-1		Experiment 1.1-2		Experiment 1.1-3	
	CR_{wl} (mm/y)	CR_{ec} (mm/y)	CR_{wl} (mm/y)	CR_{ec} (mm/y)	CR_{wl} (mm/y)	CR_{ec} (mm/y)
1	1.842	7.742	14.504	12.923	0.465	3.128
2		1.512	2.964	1.669	SEM	3.236
3		1.329	3.282	1.462	SEM	3.048
4		1.267	3.070	1.397	0.465	2.951
5		0.439	3.702	0.953	0.574	2.096
6		0.456	4.899	1.327	SEM	2.362
7	SEM	0.445	0.218	0.680	0.287	1.677
8		0.189	2.722	0.739	0.191	1.439

The time of exposure in Experiments 1.1-1, 1.1-2, and 1.1-3 was 75, 29, and 33 h, respectively.

products (Experiment 1.1-2). These errors were to a large extent corrected in the subsequent series of experiments.

3.3.1. SEM

One electrode (electrode 7) from Experiment 1.1-1 and three electrodes (electrodes 2, 3, and 6) from Experiment 1.1-3 were examined by SEM as indicated in Table 4. They were previously mounted in epoxy to avoid any damage to the surface film. The surfaces of electrodes 2 and 3 was examined as shown in Figs. 8 and 9, respectively, while the
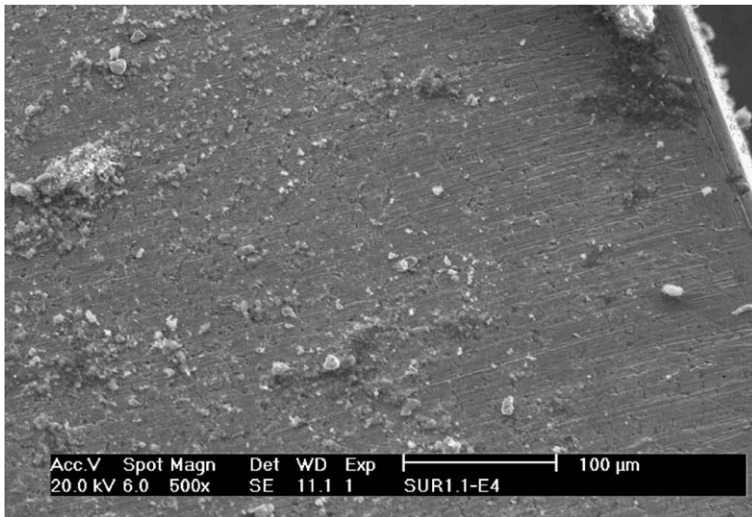

Fig. 8. SEM image of the surface of electrode 2, Experiment 1.1-3.
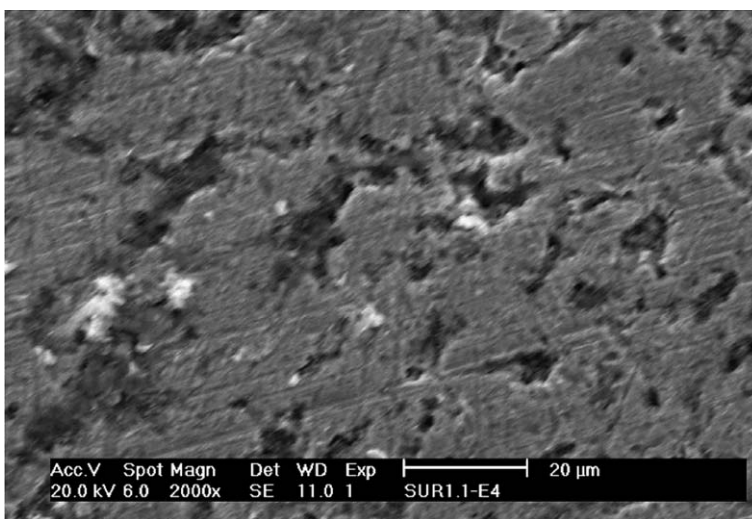
Fig. 9. SEM image of the surface of electrode 3, Experiment 1.1-3.

cross-sections of electrodes 6 and 7 were examined as shown in Figs. 10 and 11, respectively. The surface of electrodes 2 and 3 appeared to be film-free and somewhat rough. The cross-section view of electrodes 6 and 7 shows no visible film while the surface is rough and has some pits. Since all electrodes were passive and had almost the same corrosion rate at the end of the experiments, it is most likely that the protection was provided by a very thin passive film on the steel surface undetectable with SEM. The pitting may be related to the presence of chlorides.
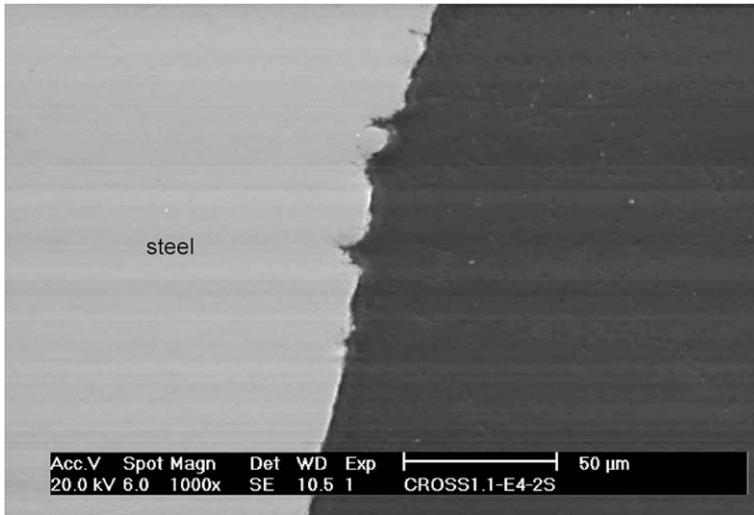
Fig. 10. SEM image of the cross-section of electrode 6, Experiment 1.1-3.
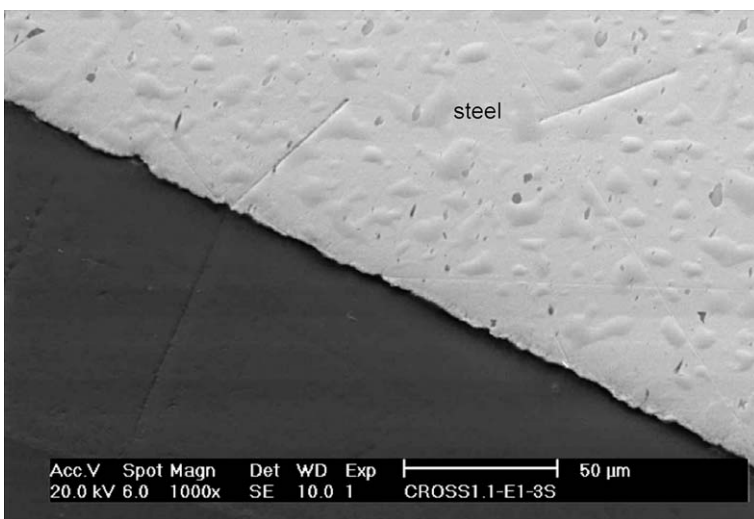
Fig. 11. SEM image of the cross-section of electrode 7, Experiment 1.1-1.

3.4. Time series

The measured corrosion rate and corrosion potential were plotted vs. time for electrode 1 in Figs. 12 and 13, respectively. The same is done for the other seven electrodes in
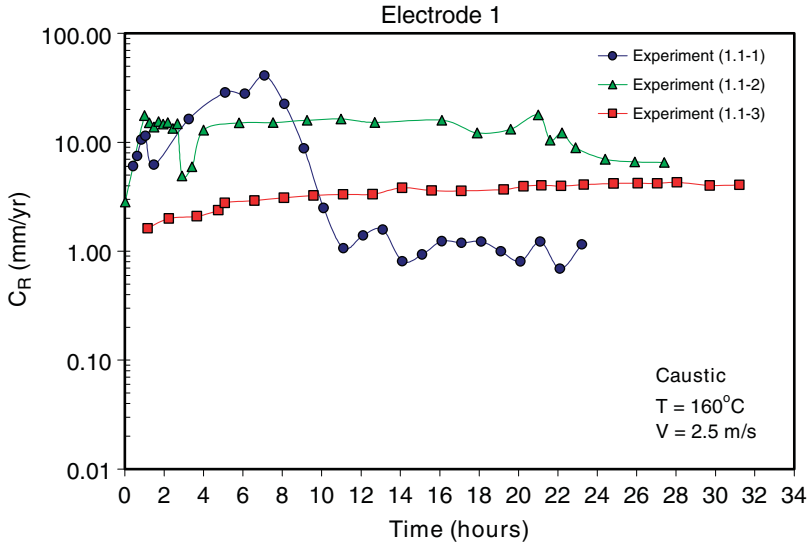
Fig. 12. Corrosion rate vs. time for electrode 1, Experiment 1.1. For the position of electrode in the test section see Fig. 2.
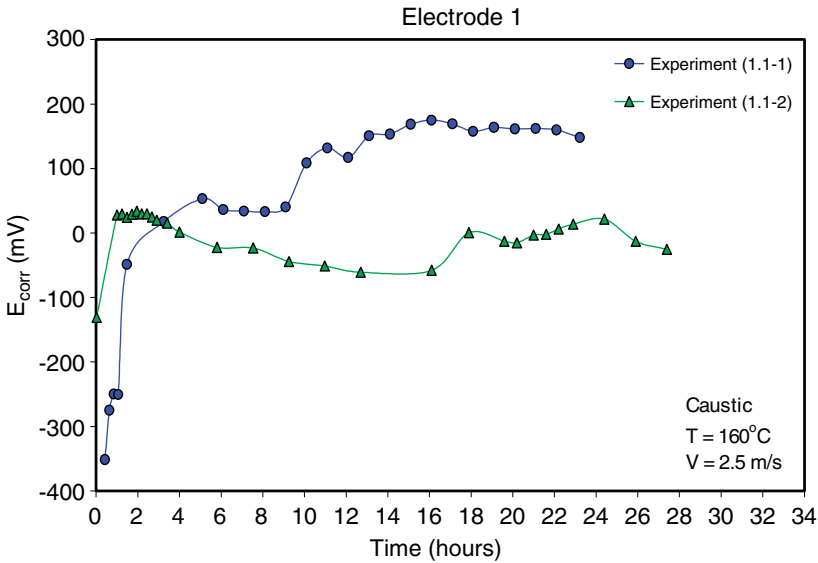
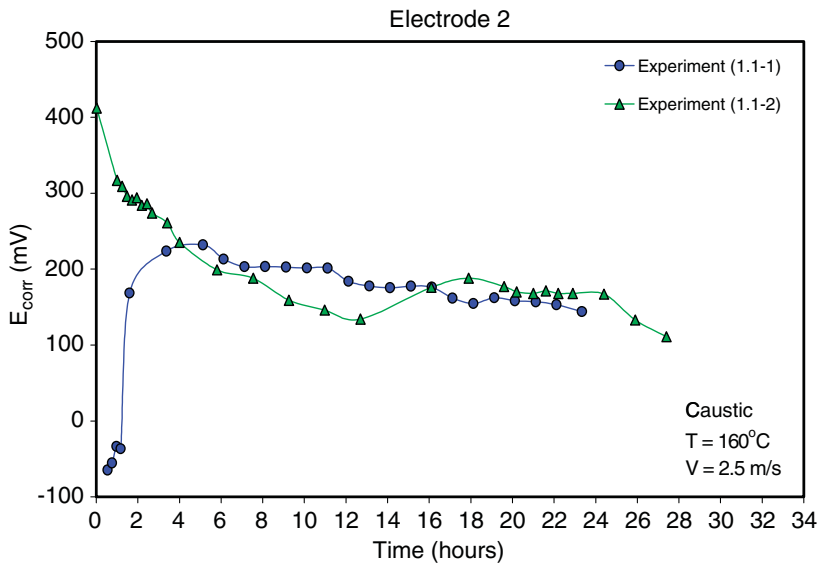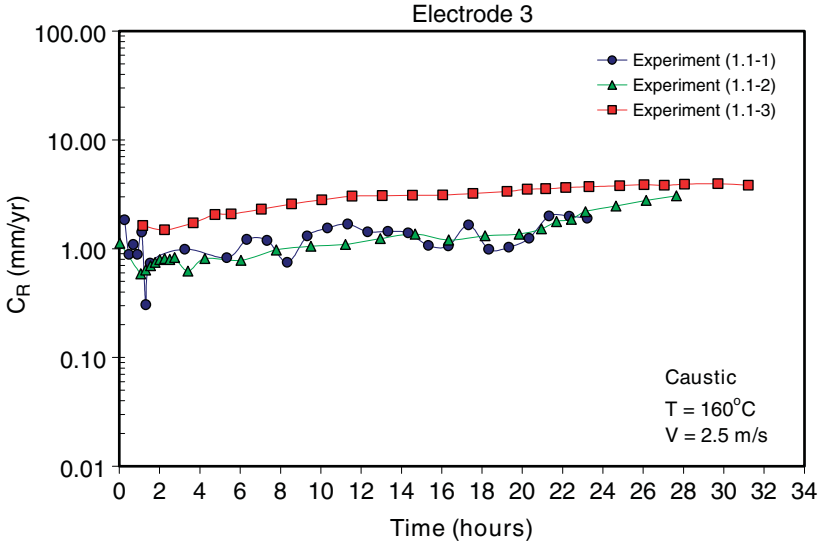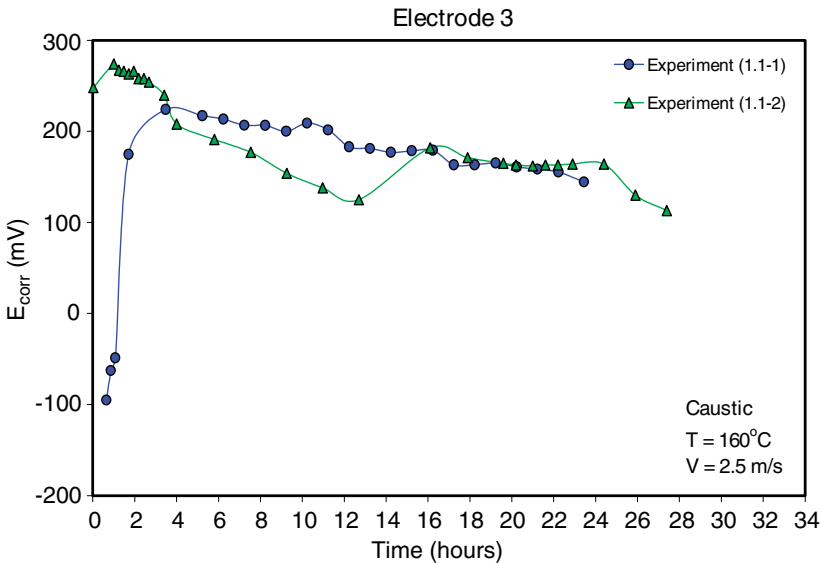Fig. 13. Corrosion potential vs. time for electrode 1, Experiment 1.1. For the position of electrode in the test section see Fig. 2.

Figs. 14–27. In each plot three repeats of the same experiment are shown for the corrosion rate and two for the potential. It is worth mentioning that the corrosion potential scale in these and all similar plots is arbitrary as the exact relationship of this scale with a standard
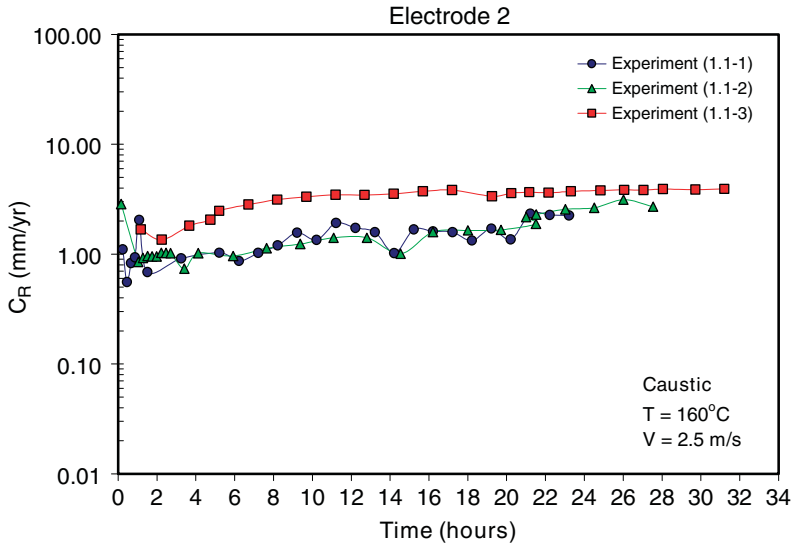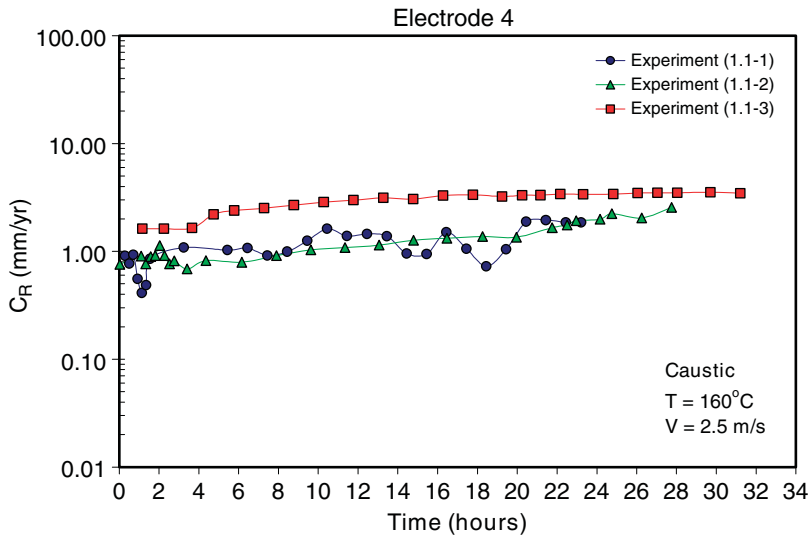

Fig. 14. Corrosion rate vs. time for electrode 2, Experiment 1.1. For the position of electrode in the test section see Fig. 2.
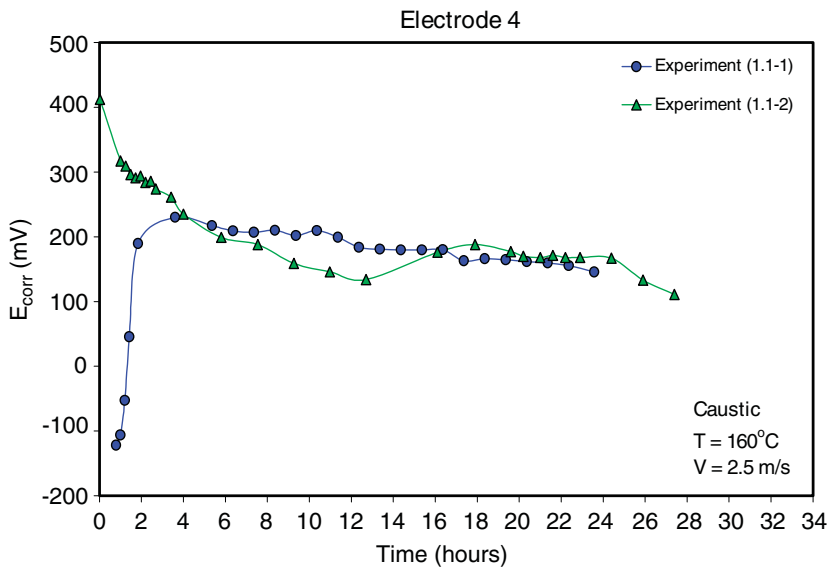

Fig. 15. Corrosion potential vs. time for electrode 2, Experiment 1.1. For the position of electrode in the test section see Fig. 2.

Ag/AgCl or any other reference potential has not been established. From the plots, the following observations can be made.

Fig. 16. Corrosion rate vs. time for electrode 3, Experiment 1.1. For the position of electrode in the test section see Fig. 2.

Fig. 17. Corrosion potential vs. time for electrode 3, Experiment 1.1. For the position of electrode in the test section see Fig. 2.

- In most cases the final corrosion rate (measured at the end of experiments) varied between 1 and 4 mm/y. This behaviour can be termed below as "passive" corrosion even if the corrosion rates are rather high, in order to contrast it to "active" corrosion when the corrosion rates were extremely high (10–100 mm/y).

Fig. 18. Corrosion rate vs. time for electrode 4, Experiment 1.1. For the position of electrode in the test section see Fig. 2.

Fig. 19. Corrosion potential vs. time for electrode 4, Experiment 1.1. For the position of electrode in the test section see Fig. 2.

- Overall there were no major differences in the final corrosion rates, measured at the end of different experiment repeats, across the eight working electrodes. However, some effect of flow on corrosion rates was seen. The corrosion rates varied between 2 and 4 mm/y for the higher velocity section and between 1 and 2 mm/y for the lower velocity section.
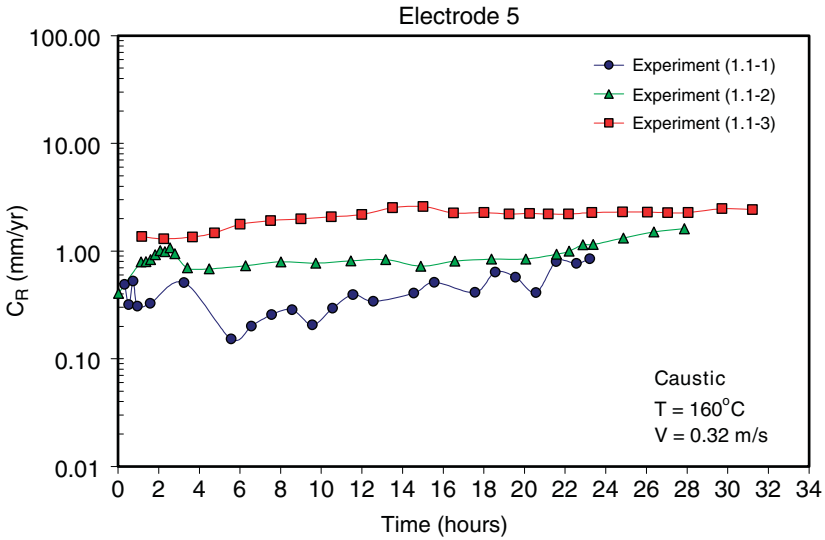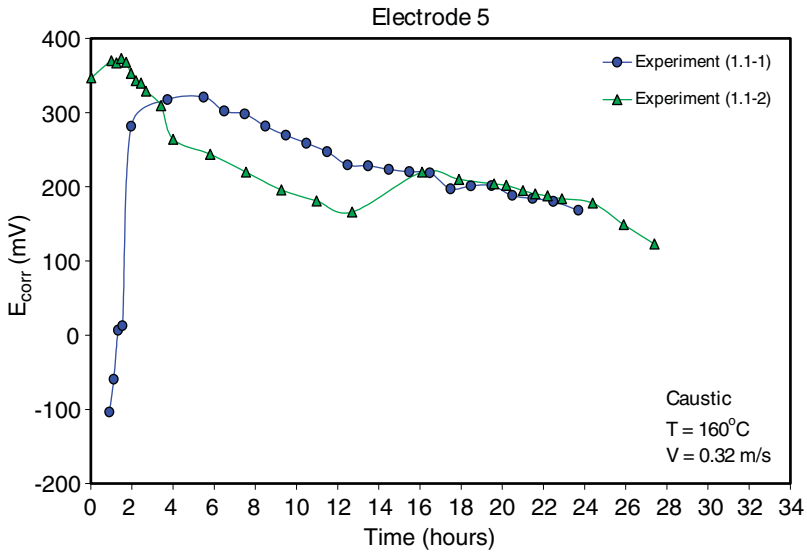

Fig. 20. Corrosion rate vs. time for electrode 5, Experiment 1.1. For the position of electrode in the test section see Fig. 2.

Fig. 21. Corrosion potential vs. time for electrode 5, Experiment 1.1. For the position of electrode in the test section see Fig. 2.

- There were significant variations of the corrosion rate at the beginning of different repeats of the same experiment, i.e. the time it took the electrodes to passivate varied across different experiment repeats, indicating that this process is difficult to control. Even if it is not shown in these plots, it was later discovered (see Part II of this study) that most caustic experiments started out with a very high corrosion rate, typically
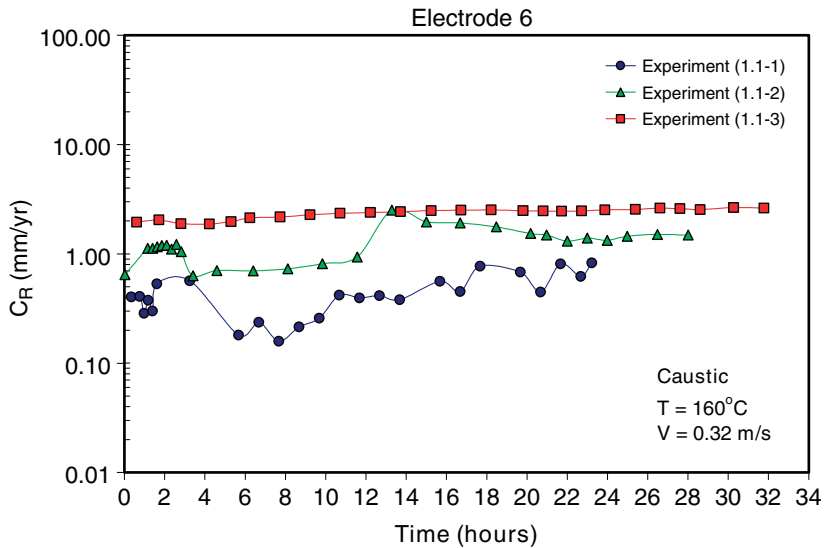

Fig. 22. Corrosion rate vs. time for electrode 6, Experiment 1.1. For the position of electrode in the test section see Fig. 2.
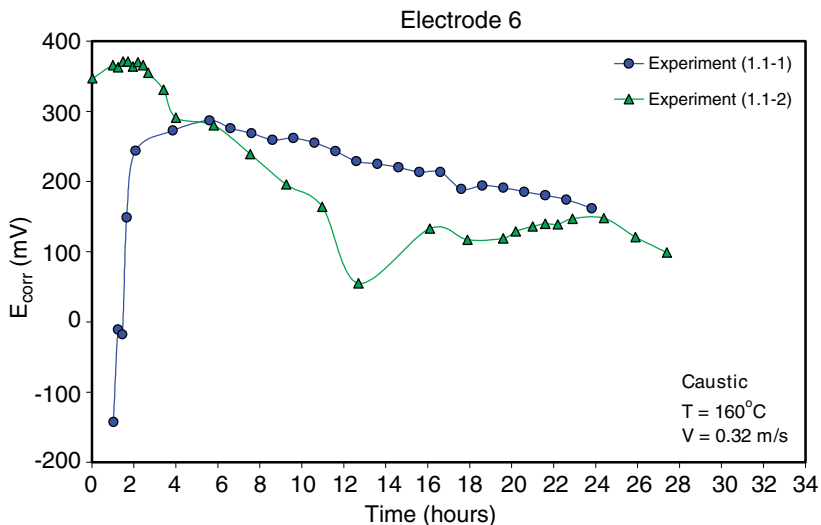

Fig. 23. Corrosion potential vs. time for electrode 6, Experiment 1.1. For the position of electrode in the test section see Fig. 2.

10–100 mm/y. The reason that this behaviour was not recorded in this series of experiments is the data logging equipment which was not started soon enough and "missed" the high corrosion rates present at the very beginning of the experiments.

- In most experiments passivation happened within the first couple hours of the experiment. There were exceptions: electrode 1 in Experiments 1.1-1 took almost 12 h to pas-
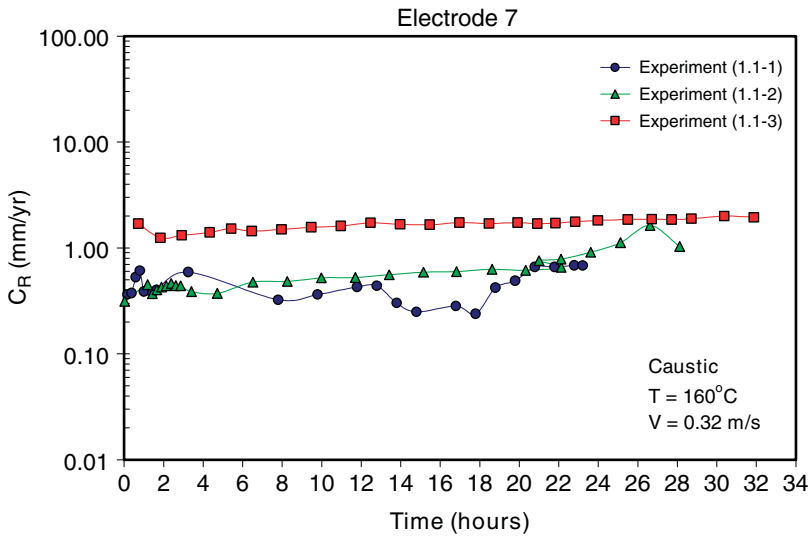

Fig. 24. Corrosion rate vs. time for electrode 7, Experiment 1.1. For the position of electrode in the test section see Fig. 2.
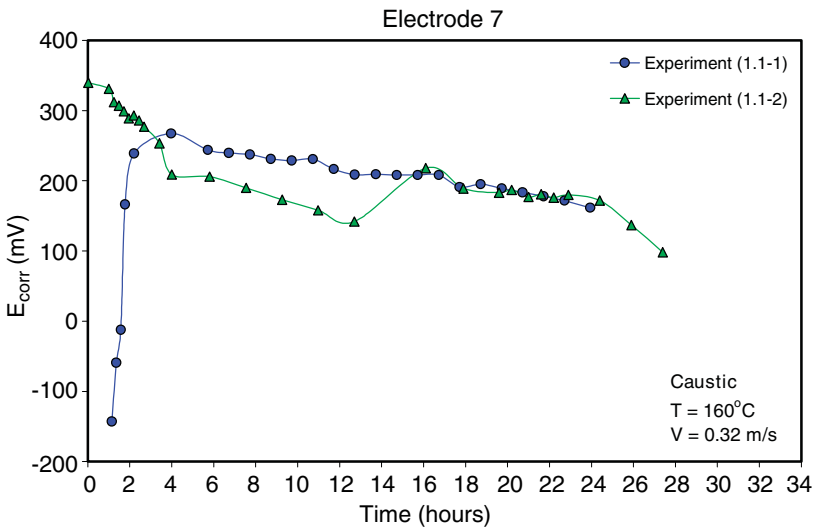

Fig. 25. Corrosion potential vs. time for electrode 7, Experiment 1.1. For the position of electrode in the test section see Fig. 2.

sivate after corroding at a very high rate (20–60 mm/y). The same electrode 1 in the repeated Experiment 1.1-2 corroded for over 20 h at approximately 10 mm/y before it passivated (see Fig. 12).
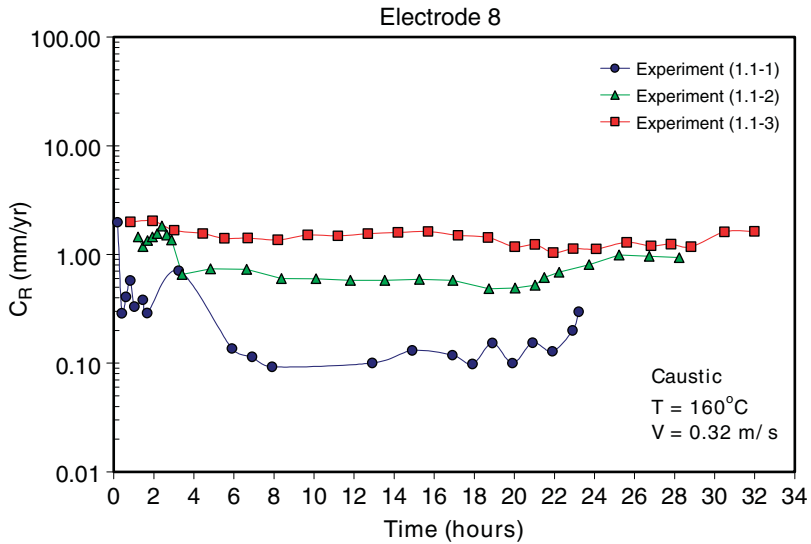

Fig. 26. Corrosion rate vs. time for electrode 8, Experiment 1.1. For the position of electrode in the test section see Fig. 2.
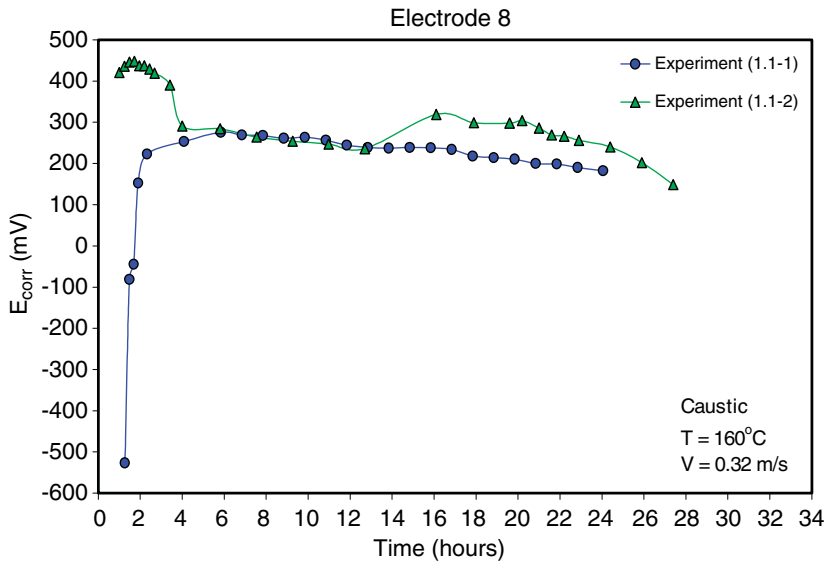

Fig. 27. Corrosion potential vs. time for electrode 8, Experiment 1.1. For the position of electrode in the test section see Fig. 2.

- The corrosion potentials support these observations. In most experiments the passivation process can be identified by the rapid increase in the corrosion potential. The potential rose typically 400 mV as the electrodes went through the active/passive transition. Again, the exception is electrode 1 (see Fig. 13).
- It can also be speculated that the unusual behavior of electrode 1 can be attributed to the disturbed turbulent flow conditions, as this electrode positioned at the inlet section of the sudden constriction (see Fig. 2) experiences the most ''violent'' i.e. turbulent flow conditions. Otherwise there was little difference in the corrosion behaviour of the remaining seven electrodes.

4. Conclusions

The aim of this research project was to investigate the erosion–corrosion of mild steel in caustic solutions with respect to the metal loss problem found in the bauxite refineries' mild steel heat exchangers. Some of the most important findings are summarized below.

- When freshly ground mild steel coupon were exposed to hot caustic the measured corrosion rate was typically 1–4 mm/y. It is speculated that the initial corrosion rate was higher but was quickly reduced due to the formation of passive surface films.
- There were rare exceptions when some electrodes experienced extended periods of very high corrosion rates (i.e. failed to passivate rapidly). They were located at the inlet section of the sudden pipe constriction where very unsteady highly turbulent flow is present. Nevertheless, the effect appeared only in a small fraction of the cases, almost at random.

References

[1] U.R. Evans, The Corrosion and Oxidation of Metals, Edward Arnold Publishers Ltd., London, 1960.
[2] G. Rocchini, Magnetite stability in aqueous solutions as a function of temperature, Corros. Sci. 36 (1994) 2043.
[3] G. Bohnsack, The Solubility of Magnetite in Water and in Aqueous Solutions of Acid and Alkali, Vulkan-Verlag, Essen, 1987.
[4] S. Giddey, D.F.A. Koch, Effect of free caustic on erosion–corrosion, Progress Reports to QAL, Part 1–3, Monash University, Melbourne, 1994–1996.
[5] S. Giddey, B. Cherry, F. Lawson, M. Forsyth, D.F.A. Koch, Corrosion of mild steel in Bayer liquor at elevated temperatures, Progress Reports to QAL, Monash University, Melbourne, 1997.
[6] F.H. Sweeton, C.F. Baes Jr., The solubility of magnetite and hydrolysis of ferrous ion in aqueous solutions at elevated temperatures, J. Chem. Thermodyn. 2 (1970) 479.
[7] R. Sriram, D. Tromans, The anodic polarization behaviour of carbon steel in hot caustic aluminate solutions, Corros. Sci. 25 (1985) 79.
[8] J. Robertson, The mechanism of high temperature aqueous corrosion of steel, Corros. Sci. 29 (1989) 1275.
[9] U. Meyer, Erosion–Corrosion in Spent Bayer Liquor, Ph.D. thesis, University of Queensland, Brisbane, 1993.
[10] W. Edwards, High Free Caustic Test Rig—Final Report, QAL Research and Development Memorandum, Reference: 20.9.1, 1995.
[11] F. Giralt, O. Trass, Mass transfer from crystalline surfaces in a turbulent impinging jet, Part I: transfer by erosion, Can. J. Chem. Eng. 53 (1975) 505.

[12] F. Giralt, O. Trass, Mass transfer from crystalline surfaces in a turbulent impinging jet, Part II: erosion and diffusional transfer, Can. J. Chem. Eng. 54 (1976) 148.
[13] U. Meyer, A. Atrens, Mater. Performance 33 (4) (1994) 57–60.
[14] U. Meyer, C.C. Brosnan, K. Bremhorst, R. Tomlins, A. Atrens, Wear 176 (1994) 163–171.
[15] U. Meyer, A. Atrens, Wear 189 (1995) 107–116.
[16] R. May, J. Orchard, Corros. Australasia 14 (1) (1988) 8–11.
[17] R. May, in: Proceedings of Conference 'Corrosion—A Tax Forever', Australian Corrosion Association, 1988, pp. 5-8.1–5-8.11.
[18] J. Flis, J.L. Dawson, J. Gill, G.C. Wood, Corros. Sci. 32 (8) (1991) 877–892.
[19] M. Yasuda, K. Fukumoto, H. Koizumi, Y. Ogata, F. Hine, Corrosion 43 (8) (1987) 492–498.
[20] Y. Ogata, H. Hori, M. Yasuda, F. Hine, J. Electrochem. Soc. 135 (1) (1988) 76–83.
[21] A.C. Makrides, N. Hackerman, J. Electrochem. Soc. 105 (1958) 156–162.
[22] D.C. Silverman, M.E. Zerr, Corrosion 42 (1986) 633–640.
[23] T. Ellison, W.R. Schmeal, J. Electrochem. Soc. 125 (1978) 524–531.
[24] T.Y. Chen, A.A. Maccari, D.D. MacDonald, Corrosion 48 (1992) 239–255.
[25] S. Zhou, M.M. Stack, R.C. Newman, Corros. Sci. 38 (1996) 1071–1084.
[26] M.M. Stack, S. Zhou, R.C. Newman, 13th ICC, Melbourne, Paper 191, 1996, pp. 1–9.
[27] N.A. Darby, C.J. Newton, J.D.B. Sharman, Light Met. (1999) 87–93.
[28] S. Giddey, B. Cherry, F. Lawson, M. Forsyth, Corros. Sci. 40 (1998) 839–842.
[29] G. Rubenis, M.Eng.Sc. thesis, University of Queensland, Australia, 1992.
[30] E.C. Potter, G.M.W. Mann, 1st Int. Cong. Metallic Corrosion, Butterworths, London, 1961, p. 417.
[31] J.E. Castle, H.G. Masterson, Corros. Sci. 6 (1966) 93–104.
[32] J.E. Castle, G.M.W. Mann, Corros. Sci. 6 (1966) 253–262.
[33] G.J. Bignold, Corros. Sci. 12 (1972) 145–154.
[34] G.J. Bignold, R. Garnsey, G.M.W. Mann, Corros. Sci. 12 (1972) 325–332.
[35] U. Meyer, A. Atrens, Mater. Performance 33 (4) (1994) 49–53.
[36] C.J. Newton, J.P. Haines, J.D.B. Sharman, D.R. Boomer, Light Met. (1998) 37–43.
[37] K. Bremhorst, J.C.S. Lai, Wear 54 (1979) 87–100.
[38] J.C.S. Lai, K. Bremhorst, Wear 54 (1979) 101–112.
[39] K. Bremhorst, P.J. Flint, Wear 145 (1991) 123–135.
[40] F. Mansfeld, Simultaneous determination of instantaneous corrosion rates and Tafel slopes from polarization resistance measurements, J. Electrochem. Soc. 120 (4) (1973) 515–518.
[41] F. Mansfeld, Tafel slopes and corrosion rates from polarization resistance measurements, Corrosion 29 (10) (1973) 397–402.
[42] Annual Book of ASTM Standards, Section 3, vol. 03.02, 1998, p. 20.
[43] Annual Book of ASTM Standards, Section 3, vol. 03.02, 1998, p. 17.